ACS APPLIED MATERIALS & INTERFACES

Research Article

www.acsami.org

Metal-Induced Crystallization of Highly Corrugated Silicon Thick Films as Potential Anodes for Li-Ion Batteries

Fei Qu,[‡] Chilin Li,*[,†] Zumin Wang,[§] Horst P. Strunk,[‡] and Joachim Maier[∥]

[†]State Key Laboratory of High Performance Ceramics and Superfine Microstructure, Shanghai Institute of Ceramics, Chinese Academy of Sciences, Shanghai 200050, China

[‡]Institute of Material Science, Chair of Material Physics, University of Stuttgart, 70569 Stuttgart, Germany

[§]Max Planck Institute for Intelligent Systems, 70569 Stuttgart, Germany

[∥]Max Planck Institute for Solid State Research, 70569 Stuttgart, Germany

Supporting Information

ABSTRACT: Silicon has turned into one of the most promising anodes for high energy rechargeable Li-ion batteries. However, a huge volume expansion during alloying with Li always induces serious pulverization/delamination for microsized electrodes as well as undesired accumulation of solid electrolyte interphase (SEI). Many efforts have focused on various nanoengineering and binding strategies to construct integrated, robust ionic/electronic wiring networks but with a trade-off between active/inactive material ratio and performance retention. Here, we first apply a metal-induced crystallization (AIC) principle for immiscible metal/semiconductor systems (Si/Al bilayers in this work) to prepare microthick Si films consisting of a high density of isolated nanocolumns. This method furthermore brings about low temperature crystallization of initial amorphous Si and conformal coating of ion-conductive oxide to enhance the Li transport kinetics of bulk and interface. Both highly satisfactory capacity retention (1650 mAh/g after 500 cycles) and rate performance (~1000 mAh/g at 8C) are achieved for such thick Si film anodes. This methodology can be used to prepare thick film samples with well-defined nanostructures but free of extra binder and conductive additives. It enables much higher area specific capacity than for inactive-component contained slurry samples and thin film samples. This postdeposition pore-creating can be extended to more alloying or conversion electrodes of thick films for high capacity Li/Na ion batteries.

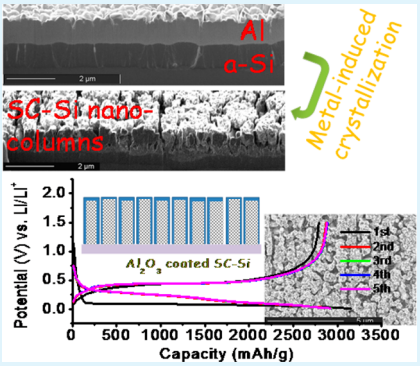

KEYWORDS: *metal-induced crystallization, nanoarchitecture, thick films, silicon anodes, lithium ion batteries*

INTRODUCTION

To meet the demands with respect to increased energy and power densities of Li-ion batteries (e.g. for potential applications in hybrid electric vehicles (HEV) and plug-in HEV (PHEV)), high capacity electrodes are required.[1,2] On the negative electrode side, silicon-based materials as typical alloy anodes are top candidates owing to the extremely high theoretical capacity of 4200 mAh/g (based on the formation of $Li_{22}Si_5$ phase) exceeding that of the widely used graphite insertion anode (372 mAh/g) by more than a factor of 10.[3] However, from Si to $Li_{22}Si_5$, a huge volume expansion ratio of ~400 % (or ~300 % for amorphous Si) occurs, typically leading to electrode pulverization/delamination, electrical contact loss, increased formation of solid electrolyte interphase (SEI), and early capacity degradation. Si nanostructures, such as nanowires and nanoparticles, or their composites (e.g. coated by carbon or conjugated polymer, alloying with inactive metal) with well-defined morphologies or ionic/electronic wiring networks have been exploited to address these problems.[4−9] Other strategies are to use more effective binders/additives, such as carboxymethyl cellulose (CMC), polyacrylic acid (PAA), and fluoroethylene carbonate (FEC), as well as flexible or nanotexture current collectors to strengthen the electrical contact, produce more stable SEI, and improve the capacity retention.[10−12]

To improve the practical energy density of Li-ion batteries, an alternative method is to reduce the amount of inactive components during electrode preparation. For example, Si thin film architectures without the usage of binders and additional conductive substances have been reported, which show near-theoretical capacity with good cyclability as long as the film thickness is below the critical cracking value of ~300 nm to prevent delamination or fracture of thin films from substrates during lithiation-driven volume expansion.[13,14] Otherwise, the capacity fades seriously after several cycles with repeating volume expansion and contraction as observed in 1 μm thick samples.[14] In view of practical application, microsized Si thick films are required to achieve high area specific capacity, and still, most of the methods previously focused on the fabrication of state-of-the-art nanocomposites by using slurrying and

Received: March 17, 2014
Accepted: May 5, 2014
Published: May 5, 2014

   dx.doi.org/10.1021/am501570w | ACS Appl. Mater. Interfaces 2014, 6, 8782−8788

pasting processes. The large-scale deposition of nanoarchitecture Si thick films (thickness >1μm) without mixing with binder and conductive additives remains a significant challenge.[15] On the other hand, in order to overcome the low coulomb efficiency caused by an unstable inherent SEI, surface coating to create an artificial passivation layer on Si has proved to be an effective approach.[16] However, many processes such as precipitation and sol-gel methods are prone to create inhomogeneous or thick insulating layers. Most recently, atomic layer deposition (ALD) successfully enabled a conformal Al_2O_3 coating with controllable nanometer thickness, which has been widely regarded as a Li-ion transport layer (especially after electrochemical lithiation to form Li−Al−O) without serious trade-off of electronic conductivity in electrode networks.[16,17] However, simple and low-cost methods for conformal coating are still lacking.

Metal induced crystallization of amorphous Si (a-Si) films, mostly by use of an Al layer, has attracted considerable interest in recent decades (for a model of the process see ref 18). This interest has been triggered by the opening chance to use the resulting thin continuous (compact) layers as seeds for epitaxial thickening to a few tens of micrometers. Such thick films are considered promising candidates for crystalline silicon solar cell films.[19] However, these seed layers up to now contain too many grain boundaries that seriously reduce the efficiencies of the produced cells.[20] In this work, we show that the metal-induced crystallization process can also be tailored to produce Si layers with a surface corrugated to a desirable degree. As a matter of fact, appropriate conduction of the crystallization process of the initially amorphous layer results in a finely structured corrugation resembling an arrangement of nanocolumns. Its large effective surface makes the resulting Si layers prospective candidates as anode materials in secondary Li-ion batteries because of its accessibility by Li ions. In addition, the nanocolumn structure can effectively accommodate volume changes and alleviate strain that may occur in the Si film during charging and discharging. In contrast to the preparation of semiconductor nanostructures by metal-catalyzed growth at high temperature, e.g. via vapor-liquid-solid (VLS) mechanism, this method allows a growth (crystallization) temperature much lower than the eutectic one (577 °C) without remarkable solubility and diffusivity in the bulk of metal catalyst. Furthermore, this process can comprise a conformal coating of Al_2O_3 which can be generated on almost each Si nanocolumn. Such nanoengineered Si films are significantly beneficial to the Li-storage kinetics as indicated so far by a reversible capacity as large as ∼1650 mAh/g with a ∼99% coulomb efficiency still after an extremely long cycling of 500 times. The microstructure evolution of Si thick films, which is dependent on the annealing temperature, annealing time, and substrate type, has been discussed on the basis of the thermodynamics and kinetics of the aluminum-induced crystallization (AIC) process in immiscible metal/semiconductor systems.[21,22] In contrast to previous utilization of complete layer exchange in Si/Al bilayers to fabricate large grain-sized Si films with high crystallinity,[23] our nanoengineering method is characterized by incomplete layer exchange and phase separation between Al and Si phases.

EXPERIMENTAL SECTION

Sample Preparation. Pure titanium foils (99.6%, Goodfellow) are used as substrates for growing Si/Al bilayers. The Ti foils were cleaned with ethanol in ultrasonic cleaner to remove organic contaminants on the surface before film growth. The Si/Al bilayer samples were prepared by sequentially sputtering Si target and Al target in a high-vacuum multitarget DC sputtering system. After reaching a background vacuum pressure less than 1×10^{-7} mbar, the substrates were cleaned with Ar^+ ions for 1 min. Then a 1500 nm thick Si layer was deposited by using a sputtering power of 100 W in an Ar atmosphere of $5.9 \cdot 10^{-3}$ mbar, followed by depositing a 1500 nm thick Al layer at a power of 200 W under the same Ar pressure. The substrate was kept at room temperature during the layer growth. The deposited Si/Al samples were then annealed in a vacuum oven at different temperatures for different times, e.g. 450 °C for 30 min as optimized conditions. The annealed samples were further etched by 1 mol/L NaOH solution to remove Al, which serves as sacrificial template. Finally they were flushed with distilled water and dried with heated Ar. The mass of final SC-Si film (0.15 mg on a substrate with the size of 5 mm × 10 mm) is obtained by comparing the weight of final sample and bare substrate. The loss amount of Si (∼50 %) is obtained by comparing the weight of pristine a-Si sample and final SC-Si sample.

Material Characterization. To observe the formation process of nanostructured Si thick film samples, their cross sections at different anneal/etch stages were observed in a focused ion beam (FIB) microscope (FEI FIB200). The surface morphology and microstructure of samples were also observed through the scanning electron microscope (SEM, Carl Zeiss Leo 1530 VP Gemini). The microstructures of the Al sublayer before annealing, e.g. via grain size statistics and grain orientation mapping, were investigated by using an electron backscattering diffraction (EBSD, Oxford, HKL) detector, which was mounted on SEM setup. X-ray diffraction (XRD) measurements of the samples were carried out in a Philps ẌPert MRD Pro diffractometer. The surface and subsurface compositions of the etched samples were analyzed by X-ray photoelectron spectroscopy (XPS, Thermo VG, Thetaprobe 300 system) in combination with *in situ* Ar^+ sputter cleaning. Two-electrode Swagelok-type cells were assembled with Si thick film samples treated in different ways as working electrodes and high-purity lithium foil (Aldrich) as counter electrode. Glass fiber (GF/D) from Whatman was employed as the separator. 1 M $LiPF_6$ in a nonaqueous mixture of ethylene carbonate (EC) and dimethyl carbonate (DMC) with a volume ratio of 1:1 (Ube Industries Ltd) was used as electrolyte. The cells were assembled in an Ar-filled glove box. Charge−discharge measurements were performed at room temperature under different rates from 0.1C to 8C (1C denotes the current density to theoretically achieve multielectron reaction to form $Li_{22}Si_5$ phase within 1 h) in a voltage range of 0.01−1.5 V on an Arbin MSTAT battery test system.

RESULTS AND DISCUSSION

The processing steps to fabricate a Si thick film with nanocolumnar morphology are sketched in Figure 1. Figure 2 shows the corresponding cross-sectional and top-view microstructures by focused ion beam microscopy (FIB) and scanning electron microscopy (SEM) . The initial amorphous Si/crystalline Al bilayer a-Si/c-Al with Al sublayer on top, each sublayer with thickness of 1.5 μm, was sputtered on a polished Ti foil substrate at room temperature in a high-vacuum multitarget DC sputtering system. The distinct interface between the Si and Al sublayers is seen from the color contrast of the FIB image (Figure 2a). The Si sublayer is amorphous as evidenced by the corresponding X-ray diffraction (XRD) analysis (Figure 3) and a smooth surface without linear corrugations typical of grain boundaries (GBs) (Figure S1). The Al overlayer displays a typical nanocrystalline microstructure with GBs and grain sizes of 300−800 nm (in the direction parallel to the surface, Figure 2a). This grain structure is indicated also by XRD analysis which reveals a dominant (111) texture. This result is further corroborated by electron backscattering diffraction (EBSD) as shown in Figure S2.

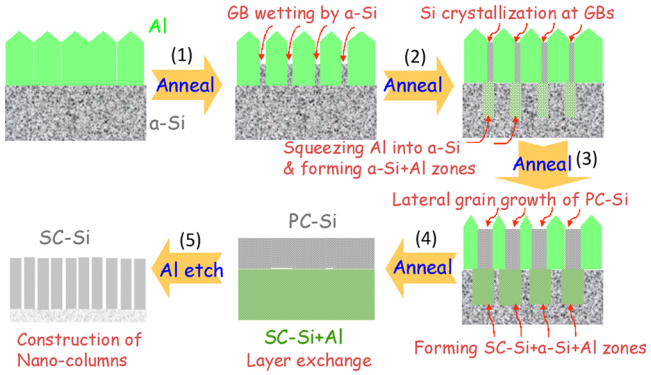

Figure 1. Scheme of annealing/etching steps to construct nanocolumnar Si thick films from Al/Si bilayers. The steps mainly include (1) Al GB wetting and splitting by a-Si, (2) crystallization of a-Si and crystalline Si growth at Al GBs, (3) transport of Al downwards into original a-Si, leading to secondary crystallization of Si therein, (4) Al-induced layer exchange, (5) etching off Al and leaving behind nanostructured Si thick films.

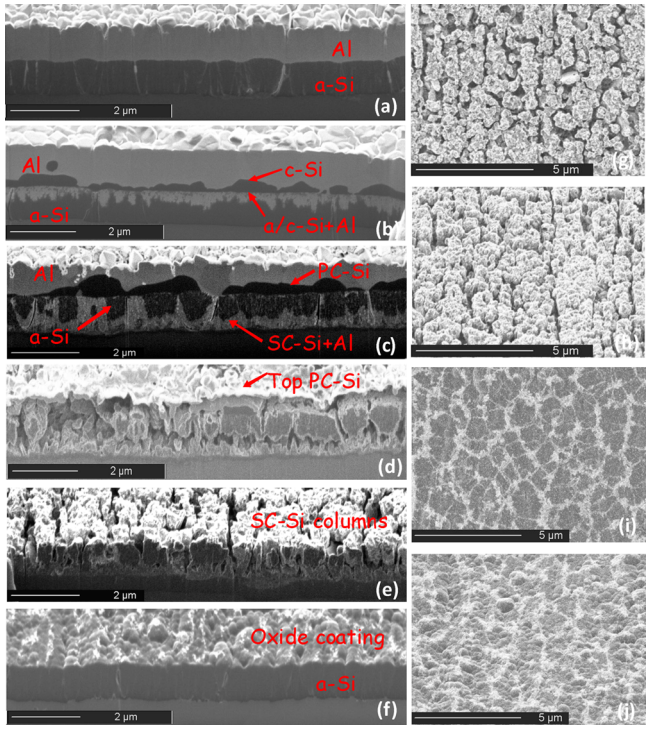

Figure 2. Cross-sectional FIB images showing (a-e) microstructural evolution from the original Al/Si bilayer to the final nanostructured Si thick film with the progress of annealing and etching, (f) Al_2O_3-coated a-Si thick film after Al etching without foregoing anneal process. Surface SEM images of Al_2O_3-coated (g) SC-Si nanocolumns and (i) a-Si thick film. SEM images of the corresponding (h) SC-Si nanocolumns and (j) a-Si thick film with a 45° tilt.

Bilayer samples of this type were annealed in a vacuum well below the eutectic temperature (450 °C for 30 min). The structural state of the samples after anneal start is shortly depicted in Figure 2b. An intermediate Si layer has formed already, indicated by the dark contrast areas, which is at least partly crystalline according to XRD. Vice versa the Al has penetrated into the area of the initial a-Si layer as noticeable from the gray pockets in the lower half. In fact, this range consists of a mixture of tiny volumes of partly crystallized Si

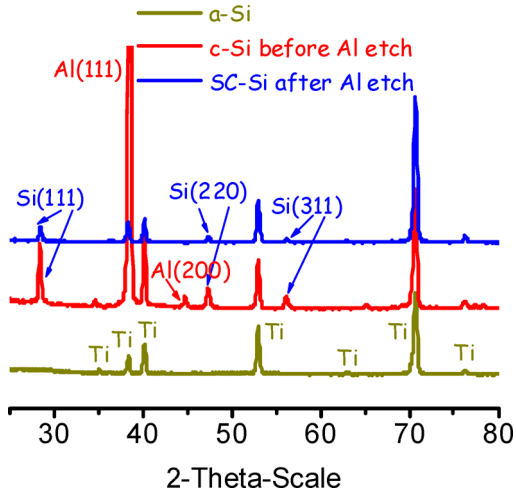

Figure 3. XRD patterns of a-Si thick film (dark yellow), Al/Si bilayer after anneal at 450 °C for 30 min (red), and nanocolumnar SC-Si thick film after annealing and Al etching (blue) on Ti substrates. The diffraction peaks of the Ti substrate, the Al template, and the Si active material are labelled, indicating highly textured Al/Si systems with a (111) grain orientation.

and Al. Note that the a-Si crystallizes this way at comparably low annealing temperature (here at 450 °C). (Solid phase crystallization of pure a-Si normally occurs at a much higher temperature of ~700 °C.[18]) These changes in the bilayer structure indicate that Si has diffused upwards into the Al layer, likely along the Al GBs and crystallize there (Figure 2b and c). This local increase in material amount squeezes Al downwards into the original a-Si sublayer where the a-Si layer also starts to crystallize (one may also discuss these processes in terms of coupled diffusional Si- and Al-fluxes).

On further annealing, this intermixing proceeds until Si- and Al-layers are progressively exchanged. At a certain stage, a discontinuous c-Si layer has formed above the original a-Si sublayer (called the primary crystallized Si, PC-Si) as shown in Figure 2d. This layer is only loosely connected to the substrate-attached silicon by statistically distributed 'bridges'. Application of an etch solution removes practically all of the Al (Figure 2d) as indicated by the absence of Al diffraction peaks in XRD (Figure 3, upper blue curve). The remaining frail Si layer is easily removed by washing with distilled water, probably aided by the development of a compressive stress field as outlined below. A final nanocolumnar architecture is left (called the secondary crystallized Si, SC-Si) attached to the Ti substrate as shown in Figure 2e,g,h. As indicated by the weak and broad Si diffraction peaks in the XRD pattern in Figure 3 (upper blue curve), this remaining Si material has a nanocrystalline structure.

All these phenomena can basically be understood in terms of the catalytic model as developed by Wang et al.[21,24] The Si atoms at the a-Si/c-Al interface can, because of a weaker bonding, rather easily be released and become highly mobile. Thermodynamically, these 'free' Si atoms then wet the Al GBs in the vicinity, because the total interface energy would decrease when a high angle Al GB is replaced by two a-Si/Al interphase boundaries.[21] The Al GBs are effectively split by this wetting layer (leading to compressive forces), and further Si atoms diffuse along the Al GBs. Therein, formation of c-Si nuclei from the free Si atoms is expected to be much more favorable than in the bulk Si. Crystallization of the a-Si wetting

dx.doi.org/10.1021/am501570w | ACS Appl. Mater. Interfaces 2014, 6, 8782−8788

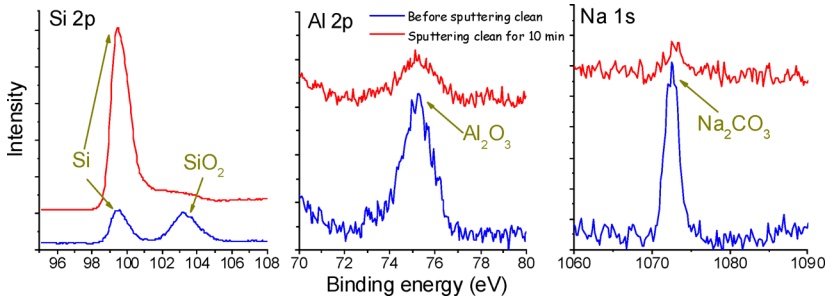

Figure 4. XPS spectra of Si 2p, Al 2p, and Na 1s of an oxide-coated a-Si thick film and that after surface sputtering clean by Ar^+ for 10 min (20 nm deep from sample surface). The oxide coating layer of about 20 nm thickness consists of components such as SiO_2, Al_2O_3, and Na_2CO_3 formed by either natural oxidation or alkali etching.

layer can occur upon reaching a critical thickness, thus causing a c-Si coverage to form at the Al GBs. Note that a thermodynamic analysis shows that crystallization of a-Si would not occur at the a-Si/Al interface.[21]

Concurrently, supported by the developing compressive forces, Al also continuously moves into the initial a-Si sublayer.[25] One can note two coupled diffusion fluxes, one Si upwards leaving vacancies in the a-Si and Al downwards filling these vacancies plus a concentration gradient. This coupled diffusion fluxes occur with different velocity and lead to an unbalanced mass distribution which causes stress. Al transported to the Si sublayer also serves as initiation sites for the secondary crystallization of Si. These newly formed Al grains or clusters would delay the further upward diffusion of Si. Thus, a mixture of aluminum, c-Si, and a-Si, depending on temperature and duration of the anneal, appears at the initial a-Si layer as shown in the sketch in Figure 1 and, by experiment, Figure 2c.

Obviously, in all these processes, the grain size of the aluminum layer determines those of the crystallized Si: Grains in the primary c-Si layer are, due to their way of formation, determined in size by the lateral extension of the Al grains. Those in the secondary c-Si are generally much smaller, as the small Al particles there give rise to a high density of sites for nucleation of c-Si. As a consequence, the annealing temperature is another determining factor of Si grain size or more generally for morphology formation. However, the functional dependence of grain size, thus also structure/morphology, on temperature appears to be rather complicated in view of the various coupled individual kinetic formation processes (convective transport in the solid state[25]) and requires to be modeled in the future. A relatively high temperature (e.g. 450 °C) usually creates more nucleation sites and thus leads to smaller Si grains. Thus, a well-defined architecture made of SC-Si porous nanocolumns (~500 nm in width, 1500 nm in height, intercolumn spacing of ~250 nm) is achieved when their surrounding Al is etched, and the top PC-Si layer is washed off (Figure 2e,g,h, and Figure S3a,b for overview SEM images).

The nanostructural manifold achievable with this solid state silicon crystallization by changing annealing temperature and duration as well as substrate type can be demonstrated by example structures obtained with border-line processing parameters. For short annealing time (e.g. 10 min at 450 °C), the Al can only diffuse to the upper region of the a-Si sublayer and remains a distance to the substrate, leading to little layer exchange. Thus, the porous morphology can develop in the upper a-Si layer only. The bottom part of a-Si is left intact as shown in Figure S4. Even though the top PC-Si seems separated from the underlying porous region, it is difficult to wash it off, probably because the developed residual stress has not reached the level to successfully support the delamination from the a-Si sublayer. When the annealing time is rather long (1.5 h−4.5 h at 450 °C), the Si columns become much coarser, as a result of overly intermixing of Al and Si. In this case the Si columns are sparsely distributed (Figures S5 and S6). On the other hand, a considerably higher annealing temperature (e.g. 500 °C) gives rise to a porous Si architecture largely lacking well-shaped Si columns (Figure S7). The seemingly more compact microstructure is characterized by stacking faults and internal porosity and is formed due to a much higher number of nucleation sites and thus smaller Si grains created at higher temperature. Besides, other factors e.g. substrate roughness may also play an important role in the layer exchange process and thus in shaping the desired Si geometry. For example, the Si films grown on a polymer Kapton substrate are able to transform into a highly porous morphology (Figure S8).

If the Al layer is etched off already before the anneal step, unexpectedly the Si surface is quite rough as compared to a smooth one as shown for the as-deposited Si films (Figure 2f,i,j, and Figure S3c,d for overview SEM images). It is known that the oxidation reaction of Al in NaOH solution is exothermic. The locally released heat is enough to promote local diffusion at the a-Si/Al interface as indicated by the traces of the Al GBs after etching, see the white lines in Figure S3c, the morphology of which corresponds to the EBSD mapping of the Al film. This diffusion also leads to the concave-convex surface. Moreover, some residues are observed at the surface particularly at the location of the original Al GBs. In fact, X-ray photoelectron spectroscopy (XPS) shows that the composition at the pristine surface, say within the XPS information depth of a few nanometers consists of Si (99.4 eV), SiO_2 (103.3 eV, possibly formed by natural oxidation),[26] Al (75.3 eV), and Na (1072.5 eV). These signals decay away practically within 20 nm into the depth as seen from the signals taken at a respective surface exposed by 1 keV Ar^+ sputtering for 10 min, see Figure 4. As the information depth of XPS is only about 5 nm, this observation indicates the presence of a thin oxidic coating of about a few nm thickness on the surface. From the reaction with CO_2 (from ambience atmosphere) it is understandable that small amounts of Al_2O_3 and Na_2CO_3 remain at the surface after etching wash and drying in heated Ar flow.[27,28] As will be seen in the following electrochemical consideration, this oxidic layer may serve as an artificial SEI to improve the coulomb efficiency of Si anodes. It is also deducible that almost all the Si nanocolumns can be coated by thin Al_2O_3, since their construction is induced by the close contact of Si side faces with the diffused Al as the case of surface contact between Si

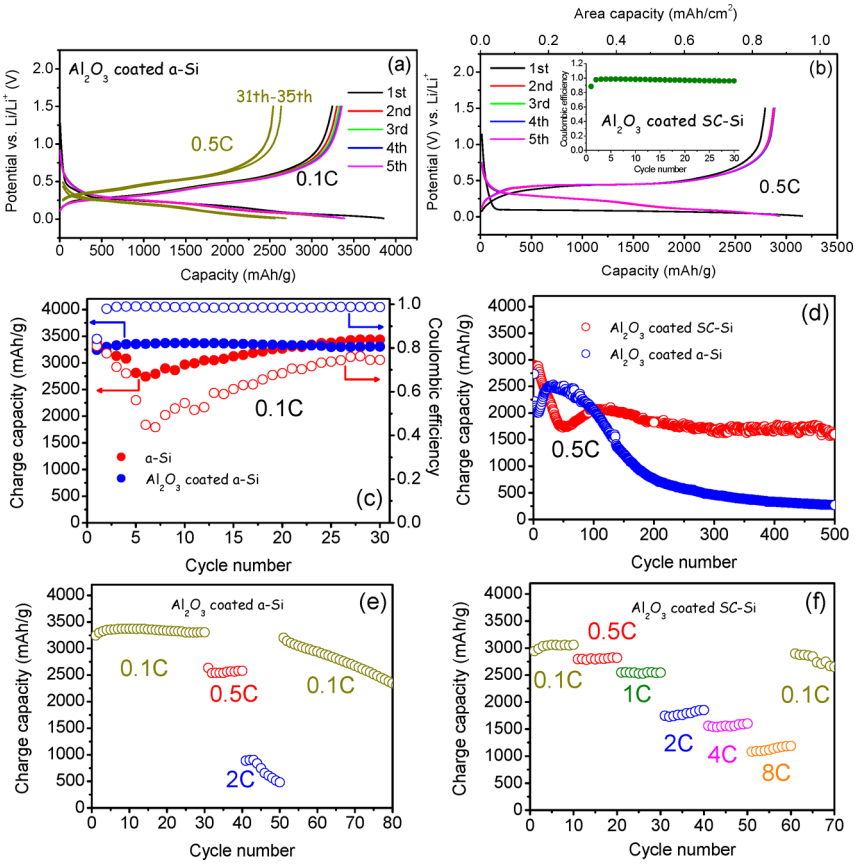

Figure 5. Voltage vs capacity profiles of Al_2O_3-coated (a) a-Si and (b) SC-Si thick films as anodes at 0.1C or 0.5 C during the first five cycles or the later cycles at 0.01−1.5 V, inset of (b) Coulombic efficiency (~98%) of a coated SC-Si thick film as a function of the cycle number at 0.5C within 30 cycles. (c) Charge capacity or coulombic efficiency of naked and coated a-Si thick films as a function of the cycle number at 0.1C within 30 cycles. (d) Charge capacity of coated a-Si and SC-Si thick films at 0.5C under a long-term cycling up to 500 cycles. Charge capacity of coated (e) a-Si and (f) SC-Si thick films at different rates from 0.1C to 8C. The capacity, cyclability, and coulombic efficiency of Si thick films greatly depend on nanoarchitecture and low-temperature crystallization as well as conformal oxide coating.

and Al mentioned above. This method may present a low-cost alternative to ALD for conformal oxide coating.

Figure 5 compares the galvanostatic performance of uncoated a-Si, Al_2O_3-coated a-Si, and Al_2O_3-coated SC-Si by using additive-free electrolyte. The SC-Si shows a typical plateau below 0.1 V during the first discharge, whereas the following discharge curves become sloped with enhanced reaction voltage ranging mostly from 0.3 to 0.01 V. These results indicate an irreversible amorphization of the c-Si during the first lithiation as reported previously.[29] In the following charge processes, it always displays plateau-like curves around 0.45 V, which is associated with the memory of original SC-Si or the preservation of local Li-insertable environment despite the macroscopic amorphization. In contrast, the a-Si always shows typical sloped discharge/charge curves for all the cycles. As known, the Li-storage kinetics and capacity could be improved by crystallizing Si as well as by downsizing Si into nanoscale so as to shorten Li diffusion length.[30] Indeed, a reversible capacity close to 3000 mAh/g (i.e. as high as 900 μAh/cm^2 or 600 μAh/cm^2-μm) at 0.5 C is achieved for Al_2O_3-coated SC-Si in the early cycles (Figure 5b), whereas for Al_2O_3-coated a-Si the capacity is 500 mAh/g lower at the same current density (Figure 5a). The coulomb efficiency of both Al_2O_3-coated samples is stabilized to 99% after the first cycle with an initial efficiency of 85−88 %, indicating that the formation of electrochemically driven SEI is effectively suppressed in view of the stable presence of Al_2O_3-contained artificial SEI. Otherwise, the coulomb efficiency for uncoated a-Si is usually much lower than 80% even though its charge capacity (~3250 mAh/g at 0.1C) and initial efficiency (80%) are comparable to that of the coated counterpart (Figure 5c and S9). The excess discharge capacity for uncoated a-Si can be attributed to the repeated formation/decomposition of SEI. Its charge capacity gradually decreases in the first five cycles and then increases until reaching to the capacity for Al_2O_3-coated a-Si. The capacity fluctuation also indicates the instability of SEI or the exposure of newly formed Si facets owing to volume change induced cracking/islanding.

Benefiting from the low temperature crystallization, conformal oxide coating, and nanoporous construction to buffer volume expansion, the SC-Si displays excellent cyclability up to 500 cycles (Figure 5d). Although there is an early capacity loss in the first 50 cycles, the capacity is then increased and stabilized at 2000 mAh/g and 1650 mAh/g (0.5C) in the following 150 and 500 cycles, respectively. The early capacity decrease is likely caused by the contact loss between the main part and the top/side edge part of SC-Si columns. The following capacity recovery can be attributed to the more exposure of newly formed Si facets to electrolyte during electrochemical activation. The good retention of capacity is also indicated by the SEM morphology after long-term cycling (Figure S10), wherein the intercolumn spaces are moderately

dx.doi.org/10.1021/am501570w | ACS Appl. Mater. Interfaces 2014, 6, 8782−8788

filled to tolerate volume extrusion. As a comparison, the capacity retention of coated a-Si is not bad in the first 100 cycles but fades quickly in the subsequent cycles and drops to 1260 mAh/g and 280 mAh/g at the 160th and 500th cycles, respectively. Likewise, the coated SC-Si shows much better rate performance than coated a-Si (Figure 5e and f). The former capacity is still preserved at about 1800 mAh/g and 1000 mAh/g when the rates are as high as 2C and 8C, respectively, whereas the latter only achieves a capacity below 1000 mAh/g at 2C. The better performance of SC-Si electrode than a-Si one is mainly ascribed to the nanoconstruction during metal-induced crystallization, which enables the effective accommodation of volume expansion with lithiation, although the original crystallinity of SC-Si is also beneficial to the kinetics of the first discharge. It was reported that high porosity coupled with the amorphous nature of Si might be helpful to reduce stresses associated with large volume changes during electrochemical lithiation/delithiation;[31] however, the attempt to fabricate nanostructured a-Si is not successful by this method. The Li-storage performance depends sensitively on annealing temperature and time (Figure S11). When overlong or overheated anneal is imposed, the capacity degrades quickly and is below 1000 mAh/g after dozens of cycles, likely due to the poor contact between intergrains or between active material and substrate as a consequence of unfavorable Al spatial distribution.

CONCLUSIONS

In summary, a novel method based on Al-induced crystallization and layer exchange in Si/Al bilayers is developed to produce nanoarchitectured Si micrometer-thick film anodes free of binder and conductive additives. A highly satisfactory retention of capacity as large as 1650 mAh/g is achievable during no less than 500 cycles. It is not only beneficial from facilitated ion/electron transport pathways and networks, volume/strain accommodation by Si crystallization and nanoengineering but also from SEI stabilization and coulomb efficiency improvement by conformal oxide coating concomitant with this methodology. It is also possible that the resultant Si is simultaneously p-doped by Al during the AIC process. Therefore, the conductivity of this Si sample is likely increased significantly.[32] This method can be extended to develop more alloy films with modulable thickness, grain size and orientation, featured texture, and configuration by accurately controlling template element diffusion and solubility for potential applications in high energy-density batteries.

ASSOCIATED CONTENT

Supporting Information

SEM and FIB images of a-Si and SC-Si thick films prepared with different annealing duration, temperature, substrate and after cycling, EBSD analysis of as-deposited Al/Si bilayer, electrochemical properties of a-Si and SC-Si prepared under nonoptimized conditions. This material is available free of charge via the Internet at http://pubs.acs.org.

AUTHOR INFORMATION

Corresponding Author

*E-mail: chilinli@mail.sic.ac.cn.

Notes

The authors declare no competing financial interest.

ACKNOWLEDGMENTS

The authors thank F. Thiele, R. Völker, and Dr. G. Richter for their technical support on sample preparation and G. Maier for XRD measurement as well as Dr. Z. H. Cui and Prof. X. X. Guo for electrochemistry measurement and reading the manuscript. C. L. Li would like to thank the "Hundred Talents" program of Chinese Academy of Sciences and the National Natural Science Foundation of China under Grant No. 51372263 for support.

REFERENCES

(1) Cabana, J.; Monconduit, L.; Larcher, D.; Palacin, M. R. Beyond Intercalation-Based Li-Ion Batteries: The State of The Art and Challenges of Electrode Materials Reacting through Conversion Reactions. *Adv. Mater.* **2010**, *22*, E170−E192.

(2) Li, H.; Wang, Z. X.; Chen, L. Q.; Huang, X. J. Research on Advanced Materials for Li-Ion Batteries. *Adv. Mater.* **2009**, *21*, 4593−4607.

(3) Yang, J.; Wang, B. F.; Wang, K.; Liu, Y.; Xie, J. Y.; Wen, Z. S. Si/C Composites for High Capacity Lithium Storage Materials. *Electrochem. Solid-State Lett.* **2003**, *6*, A154−A156.

(4) Chan, C. K.; Peng, H. L.; Liu, G.; McIlwrath, K.; Zhang, X. F.; Huggins, R. A.; Cui, Y. High Performance Lithium Battery Anodes Using Silicon Nanowires. *Nat. Nanotechnol.* **2008**, *3*, 31−35.

(5) Abel, P. R.; Lin, Y. M.; Celio, H.; Heller, A.; Mullins, C. B. Improving the Stability of Nanostructured Silicon Thin Film Lithium-Ion Battery Anodes through Their Controlled Oxidation. *ACS Nano* **2012**, *6*, 2506−2516.

(6) Kim, H.; Seo, M.; Park, M. H.; Cho, J. A Critical Size of Silicon Nano-Anodes for Lithium Rechargeable Batteries. *Angew. Chem., Int. Ed.* **2010**, *49*, 2146−2149.

(7) Xin, S.; Guo, Y. G.; Wan, L. J. Nanocarbon Networks for Advanced Rechargeable Lithium Batteries. *Acc. Chem. Res.* **2012**, *45*, 1759−1769.

(8) Cao, F. F.; Deng, J. W.; Xin, S.; Ji, H. X.; Schmidt, O. G.; Wan, L. J.; Guo, Y. G. Cu-Si Nanocable Arrays as High-Rate Anode Materials for Lithium-Ion Batteries. *Adv. Mater.* **2011**, *23*, 4415−4420.

(9) Wu, H.; Yu, G. H.; Pan, L. J.; Liu, N.; McDowell, M. T.; Bao, Z. N.; Cui, Y. Stable Li-Ion Battery Anodes by In-Situ Polymerization of Conducting Hydrogel to Conformally Coat Silicon Nanoparticles. *Nat. Commun.* **2013**, *4*, 1943.

(10) Kovalenko, I.; Zdyrko, B.; Magasinski, A.; Hertzberg, B.; Milicev, Z.; Burtovyy, R.; Luzinov, I.; Yushin, G. A Major Constituent of Brown Algae for Use in High-Capacity Li-Ion Batteries. *Science* **2011**, *334*, 75−79.

(11) Etacheri, V.; Haik, O.; Goffer, Y.; Roberts, G. A.; Stefan, I. C.; Fasching, R.; Aurbach, D. Effect of Fluoroethylene Carbonate (FEC) on The Performance and Surface Chemistry of Si-Nanowire Li-Ion Battery Anodes. *Langmuir* **2012**, *28*, 965−976.

(12) Choi, J. Y.; Lee, D. J.; Lee, Y. M.; Lee, Y. G.; Kim, K. M.; Park, J. K.; Cho, K. Y. Silicon Nanofibrils on A Flexible Current Collector for Bendable Lithium-Ion Battery Anodes. *Adv. Funct. Mater.* **2013**, *23*, 2108−2114.

(13) Ohara, S.; Suzuki, J.; Sekine, K.; Takamura, T. A Thin Film Silicon Anode for Li-Ion Batteries Having A Very Large Specific Capacity and Long Cycle Life. *J. Power Sources* **2004**, *136*, 303−306.

(14) Maranchi, J. P.; Hepp, A. F.; Kumta, P. N. High Capacity, Reversible Silicon Thin-Film Anodes for Lithium-Ion Batteries. *Electrochem. Solid-State Lett.* **2003**, *6*, A198−A201.

(15) Usui, H.; Uchida, N.; Sakaguchi, H. Influence of Order in Stepwise Electroless Deposition on Anode Properties of Thick-Film Electrodes Consisting of Si Particles Coated with Ni and Cu. *J. Power Sources* **2011**, *196*, 10244−10248.

(16) He, Y.; Yu, X. Q.; Wang, Y. H.; Li, H.; Huang, X. J. Alumina-Coated Patterned Amorphous Silicon as The Anode for A Lithium-Ion Battery with High Coulombic Efficiency. *Adv. Mater.* **2011**, *23*, 4938−4941.

(17) Scott, I. D.; Jung, Y. S.; Cavanagh, A. S.; Yan, Y. F.; Dillon, A. C.; George, S. M.; Lee, S. H. Ultrathin Coatings on Nano-$LiCoO_2$ for Li-Ion Vehicular Applications. *Nano Lett.* **2011**, *11*, 414−418.
(18) Wang, Z. M.; Jeurgens, L. P. H.; Wang, J. Y.; Mittemeijer, E. J. Fundamentals of Metal-Induced Crystallization of Amorphous Semiconductors. *Adv. Eng. Mater.* **2009**, *11*, 131−135.
(19) Bergmann, R. B.; Werner, J. H. The Future of Crystalline Silicon Films on Foreign Substrates. *Thin Solid Films* **2002**, *403-404*, 162−169.
(20) Wagner, G.; Steiner, B.; Winter, B.; Dorsch, W.; Voigt, A.; Strunk, H. P.; Brendel, R.; Wolf, M.; Werner, J. H. *Proc. 13th European PV Solar Energy Conference*, Nice, 1995; p 461.
(21) Wang, Z. M.; Wang, J. Y.; Jeurgens, L. P. H.; Mittemeijer, E. J. Thermodynamics and Mechanism of Metal-Induced Crystallization in Immiscible Alloy Systems: Experiments and Calculations on Al/a-Ge and Al/a-Si Bilayers. *Phys. Rev. B* **2008**, *77*, 045424.
(22) Wang, J. Y.; Wang, Z. M.; Mittemeijer, E. J. Mechanism of Aluminum-Induced Layer Exchange upon Low-Temperature Annealing of Amorphous Si/Polycrystalline Al Bilayers. *J. Appl. Phys.* **2007**, *102*, 113523.
(23) Jung, M.; Okada, A.; Saito, T.; Suemasu, T.; Usami, N. On the Controlling Mechanism of Preferential Orientation of Polycrystalline-Silicon Thin Films Grown by Aluminum-Induced Crystallization. *Appl. Phys. Express* **2010**, *3*, 095803.
(24) Wang, Z. M.; Gu, L.; Phillipp, F.; Wang, J. Y.; Jeurgens, L. P. H.; Mittemeijer, E. J. Metal-Catalyzed Growth of Semiconductor Nanostructures without Solubility and Diffusivity Constraints. *Adv. Mater.* **2011**, *23*, 854−859.
(25) Wang, Z. M.; Gu, L.; Jeurgens, L. P. H.; Phillipp, F.; Mittemeijer, E. J. Real-Time Visualization of Convective Transportation of Solid Materials at Nanoscale. *Nano Lett.* **2012**, *12*, 6126−6132.
(26) Philippe, B.; Dedryvere, R.; Gorgoi, M.; Rensmo, H.; Gonbeau, D.; Edstrom, K. Improved Performances of Nanosilicon Electrodes using The Salt LiFSI: A Photoelectron Spectroscopy Study. *J. Am. Chem. Soc.* **2013**, *135*, 9829−9842.
(27) Paparazzo, E. XPS, AES and EELS Studies of Al Surfaces. *Vacuum* **2001**, *62*, 47−60.
(28) Wagner, C. D.; Riggs, W. W.; Davis, L. E. *Handbook of X-ray Photoelectron Spectroscopy*; Perkin-Elmer Corp., Physical Electronics Division: Eden Prairie, MN, 1992.
(29) Limthongkul, P.; Jang, Y. I.; Dudney, N. J.; Chiang, Y. M. Electrochemically-Driven Solid-State Amorphization in Lithium-Silicon Alloys and Implications for Lithium Storage. *Acta Mater.* **2003**, *51*, 1103−1113.
(30) Liu, X. H.; Zhang, L. Q.; Zhong, L.; Liu, Y.; Zheng, H.; Wang, J. W.; Cho, J. H.; Dayeh, S. A.; Picraux, S. T.; Sullivan, J. P.; Mao, S. X.; Ye, Z. Z.; Huang, J. Y. Ultrafast Electrochemical Lithiation of Individual Si Nanowire Anodes. *Nano Lett.* **2011**, *11*, 2251−2258.
(31) Esmanski, A.; Ozin, G. A. Silicon Inverse-Opal-Based Macroporous Materials as Negative Electrodes for Lithium Ion Batteries. *Adv. Funct. Mater.* **2009**, *19*, 1999−2010.
(32) Gong, S. F.; Hentzell, H. T. G.; Robertsson, A. E.; Hultman, L.; Hörnström, S. E.; Radnoczi, G. Al-Doped and Sb-Doped Polycrystalline Silicon Obtained by Means of Metal-Induced Crystallization. *J. Appl. Phys.* **1987**, *62* (9), 3726−3732.